Journal of Biomechanics 47 (2014) 3094–3099

Contents lists available at ScienceDirect

Journal of Biomechanics

journal homepage: www.elsevier.com/locate/jbiomech
www.JBiomech.com

Mechanical properties vary for different regions of the finger extensor apparatus

Kai Qian [a], Kay Traylor [a], Sang Wook Lee [b,c], Benjamin Ellis [d], Jeffrey Weiss [d,e], Derek Kamper [a,f,*]

[a] Department of Biomedical Engineering, Illinois Institute of Technology, Wishnick Hall, Suite 314, 3255 S Dearborn St, Chicago, IL 60616, United States
[b] Department of Biomedical Engineering, Catholic University of America, Washington, DC 20064, United States
[c] Center for Applied Biomechanics and Rehabilitation Research, National Rehabilitation Hospital, Washington, DC 20010, United States
[d] Department of Bioengineering, and Scientific Computing and Imaging Institute, University of Utah, Salt Lake City, UT 84112, United States
[e] Department of Orthopedics, University of Utah, Salt Lake City, UT 84108, United States
[f] Sensory Motor Performance Program, Rehabilitation Institute of Chicago, Chicago, IL 60611, United States

ARTICLE INFO

Article history:
Accepted 21 June 2014

Keywords:
Extensor apparatus
Material properties
Soft tissue mechanics
Tensile

ABSTRACT

The extensor apparatus, an aponeurosis that covers the dorsal side of each finger, transmits force from a number of musculotendons to the phalanges. Multiple tendons integrate directly into the structure at different sites and the extensor apparatus attaches to the phalanges at multiple points. Thus, prediction of the force distribution within the extensor apparatus, or hood, and the transmission to the phalanges is challenging, especially as knowledge of the underlying mechanical properties of the tissue is limited. We undertook quantification of some of these properties through material testing of cadaver specimens. We punched samples at specified locations from 19 extensor hood specimens. Material testing was performed to failure for each sample with a custom material testing device. Testing revealed significant differences in ultimate load, ultimate strain, thickness, and tangent modulus along the length of the extensor hood. Specifically, thickness, ultimate load, and ultimate strain were greater in the more proximal sections of the extensor hood, while the tangent modulus was greater in the more distal sections. The variations in mechanical properties within the hood may impact prediction of force transmission and, thus, should be considered when modeling the action of the extensor apparatus. Across the extensor hood, tangent modulus values were substantially smaller than values reported for other soft tissues, such as the Achilles tendon and knee ligaments, while ultimate strains were much greater. Thus, the tissue in the extensor apparatus seems to have greater elasticity, which should be modeled accordingly.

1. Introduction

The extensor apparatus, or extensor hood, is a continuous aponeurosis that covers the dorsal surface of the finger phalanges from the metacarpophalangeal (MCP) joint to the distal phalanx (Tubiana and Valentin, 1964). Tendons from a number of muscles integrate into the extensor apparatus, which, in turn, inserts into the phalanges at multiple locations and has numerous other connections with the bones and skin through soft tissue (Landsmeer, 1949; Milford, 1968; Sabnis, 2013). The presence of the extensor hood, in conjunction with the series of annular and cruciform ligaments that form anatomical pulleys on the palmar surface of the phalanges (Doyle, 1988), allows transmission of force from the muscles, which all reside proximal to the MCP joint, to the segments of the finger. This configuration allows for maximization of the passive range of motion of the joints, as the muscle bellies do not restrict joint movement (i.e. in contrast to biceps brachii limiting elbow flexion, for example). In addition, the proximal location of the muscles minimizes the mass, and thus inertia, of the moving digit.

These advantages necessitate more complex musculotendon force transmission and more complicated control (Lemon, 1993; Valero-Cuevas, 2009). Depending on the digit, four or even five musculotendons (Infantolino and Challis, 2010) may integrate into the extensor hood. Force transmission through the extensor apparatus is still not well understood despite a number of studies examining the influence of the extensor hood on joint kinematics and kinetics and the localized strain developed in response to

* Corresponding Author at: Department of Biomedical Engineering, Illinois Institute of Technology, Wishnick Hall, Suite 314, 3255 S Dearborn St, Chicago, IL 60616, United States. Tel.: +1 312 567 5099; fax: +1 312 567 5707.
E-mail address: d-kamper@northwestern.edu (D. Kamper).

http://dx.doi.org/10.1016/j.jbiomech.2014.06.035
0021-9290/

applied loading. Landsmeer (1949), for example, described the anatomy of the extensor hood and its potential role for contributing to coupled joint movement within a digit (Landsmeer, 1949) and producing phenomena such as the claw hand (Mulder and Landsmeer, 1968). Micks and Reswick (1981) estimated the effective moment arm of the extensor hood at the proximal interphalangeal (PIP) joint and noted varying stresses in the extensor structure (Micks and Reswick, 1981). An et al. (1983) estimated anatomical extension moment arms for the index finger muscles, including those that merge with the extensor hood (An et al., 1983). Lee et al. (2008b) computed effective static moment arms for the extensor muscles from fingertip forces measured in response to tendon loading in cadaver specimens (Lee et al., 2008b) and Kamper et al. (2006) looked at changes in extensor moment arms with changes in posture from fingertip forces measured in vivo in response to electrical stimulation (Kamper et al., 2006). von Schroeder and Botte (1993) examined joint movement in response to loading of the extensor digitorum communis tendon (von Schroeder and Botte, 1993). While these studies contributed to understanding the behavior of the extensor hood, they did not address the underlying material properties of the structure itself.

Systematic quantification of the material properties of different regions of the extensor hood is lacking. While multiple researchers directly measured the local strain developed at different locations within the extensor apparatus in response to tendon loading using Hall-effect sensors (Hurlbut and Adams, 1995), microstrain gauges (Sarrafian et al., 1970) or optical measurements (Lee et al., 2008a), material properties such as elastic modulus, ultimate tensile strength, and ultimate strain were not directly measured. Garcia-Elias et al. (1991b) performed force-displacement measurements on intact specimens (Garcia-Elias et al., 1991b), but the connections between the extensor apparatus and surrounding structures could have influenced the input–output relationships, and stress–strain values were not reported.

These material properties are important for formulating biomechanical models created to predict the force distribution throughout the extensor hood for different tendon loading patterns. Past efforts to model the hood, beginning with the representation of a rhomboidal network of tendons (Winslow, 1732) and further refined over the past 30 years (Garcia-Elias et al., 1991b; Saxena et al., 2012; Valero-Cuevas et al., 1998; Zancolli, 1979), have of necessity assumed uniform properties throughout the extensor apparatus (Lee et al., 2008a; Valero-Cuevas et al., 1998). The extensor hood, however, is a heterogeneous structure (Garcia-Elias et al., 1991a). These heterogeneities can impact the force distribution to different bony connections, such as the central and terminal slips, with dramatic impacts on the fingertip movement or force development in response to a given tendon loading pattern. This has ramifications for the potential use of these models for helping to guide repair of extensor hood injuries, such as mallet finger (Stack, 1969) or swan neck deformity (Harrison, 1965).

Thus, the goal of this study was to investigate the mechanical properties of different segments of the extensor apparatus through tensile testing. We hypothesized that the elasticity of different portions of the apparatus would vary significantly. These data would support the development of computer models, including finite element models, to better explain the force propagation through the extensor mechanism.

2. Materials and method

2.1. Procedure

A convenience sample of 19 finger extensor hood specimens (9 index fingers: 5 from right hands and 4 from left hands, 10 middle fingers: 6 from right hands and 4 from left hands) was harvested from fresh-frozen human cadaveric hands. The specimens were dissected in one piece from all other structures, such as skin, subcutaneous tissue, and bone. The harvested specimens were frozen and then thawed immediately before testing.

Dog-bone shaped samples were taken at multiple sites within each extensor specimen. All samples were oriented along the fiber directions. Samples were obtained using a custom punch (Quapp and Weiss, 1998) resulting in a test area of roughly 10 mm × 2 mm with tabs at either end to permit clamping to a custom material testing device. Specifically, samples were taken from a set of 7 different regions: (A) proximal to the MCP joint (where the long extensor tendon merges with the hood), (B) over the MCP joint, (C) at the central band, (D) at the central slip, (E) at the terminal slip, (F) at the sagittal band, and (G) at the lateral band (see Fig. 1). The long axis of the sample was aligned with the direction of the collagen fibers (e.g. along the long axis of the finger for the central band and oblique to this axis for the sagittal band).

The tabs of each sample were wrapped in saline-moistened gauze and mounted in clamps with serrations designed to prevent tissue slippage. The initial length was determined by clamp-to-clamp distance before testing. The samples were assumed to have a rectangular cross-sectional area, and the thickness and width were measured at the central part of each sample with digital calipers (Model 500-196-20, Mitutoyo, Kawasaki-Shi, Japan). Three measurements were made for each dimension and the average value was employed. Two black 1.6-mm diameter plastic spherical markers were glued to the tissue for strain measurements, as shown in Fig. 2. The tissue samples were kept moist through repeated administration of 5% saline solution.

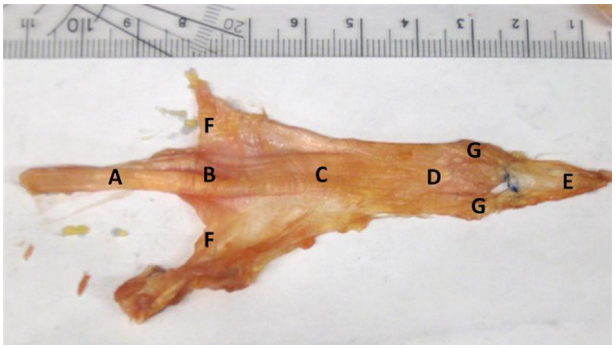

Fig. 1. Extensor hood after excision from cadaveric hand with schematic showing from where dog bone shaped tensile test specimens were taken. Sample locations: (A) proximal MCP; (B) over MCP; (C) central band; (D) central slip; (E) terminal slip; (F) sagittal band; and (G) lateral band.

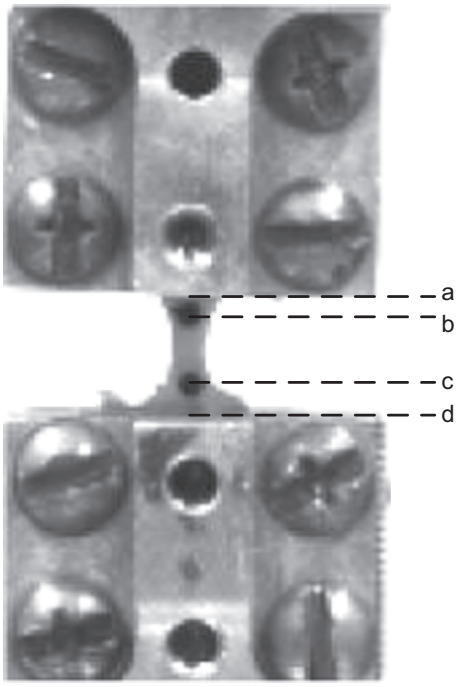

Fig. 2. Specimen sample positioned for testing within the MTS. The upper and lower clamps hold the tabs of the dog bone-shaped sample. Black markers, visible in the camera images, were affixed to the central portion of the sample as b and c in the figure. a: upper clamp edge; and d: lower clamp edge.

Biomechanical testing was conducted on a custom materials testing system (MTS), incorporating a linear actuator (RSA24; Tolomatic, Inc., Hamel, MN, USA), a brushless servomotor (MRV 21; Tolomatic, Inc., Hamel, MN, USA), a brushless servomotor drive (DV-10; Tolomatic, Inc., Hamel, MN, USA), and a load cell (Model 31, AL311BN, 50 lbs, Honeywell Sensotec, Columbus, OH, USA, accuracy $\pm 0.25\%$ FS). The specimens were loaded to failure at a rate of 0.5 mm/s. Testing was performed at room temperature and recorded by a 1 megapixel video camera (IPX-1M48-L; Imperx Inc., Boca Raton, FL, USA) with 25-mm Pentax lens (Pentax, Tokyo, Japan) using Digital Motion Analysis Software (DMAS v7, Spicatek, HI, USA, accuracy ± 0.3 mm). Time, force, and actuator displacement were recorded at 40 Hz using LabVIEW data acquisition software (National Instruments, Austin, TX, USA) synchronized with video image recording.

2.2. Analysis

Load–displacement curves, using the clamp displacement, were first generated to align the different trials. The point on the curve at which the load first rose from the baseline value was identified manually and designated as the point of zero load and zero displacement. Load and displacement were subsequently measured from this point. Marker position data, synched with the force and clamp displacement data from the MTS, were extracted from the recorded video after testing by the Digital Motion Analysis Software. The nominal stress was determined by dividing the force output from the MTS load cell by the initial cross-sectional area of the sample, as determined from the caliper measurements of width and thickness. Soft tissue strain is typically measured by one of two means, either from the displacement of the MTS (thereby recording the clamp-to-clamp nominal strain, or "clamp strain" for the specimen (Woo et al., 1983)) or from optical data recording the measurement of traceable markers attached to the specimen, (the imaging stretch (Kelleher et al., 2011) or "local" strain (Butler et al., 1984)). As both techniques have relative pros and cons, and as the mechanical tissue properties determined from the two different methods may vary (Butler et al., 1984; Kelleher et al., 2011), we provide both sets of values for completeness. Clamp nominal strain was computed by dividing the relative actuator displacement, measured by the motor's encoder, by specimen length at zero displacement. Local nominal strain was obtained from the marker displacement as recorded by the camera. As tissue failure did not always occur between the two markers, the displacement used to compute local strain was chosen to coincide with the location of the tissue failure: (1) displacement between the markers (b and c, in Fig. 2) when failure occurred in this region; (2) displacement between upper clamp edge a and lower marker c when failure occurred above b; (3) displacement between upper marker b and lower clamp edge d when specimen failure occurred below marker c. Ultimate clamp and local strains were determined at the time of ultimate stress. The clamp and local tangent moduli were computed as the slope derived from linear regression performed along the linear portion of the respective stress–strain curves (see Fig. 3). Linear stiffness was estimated from clamp tangent moduli by multiplying clamp moduli by specimen cross section area and divided by specimen length at zero displacement.

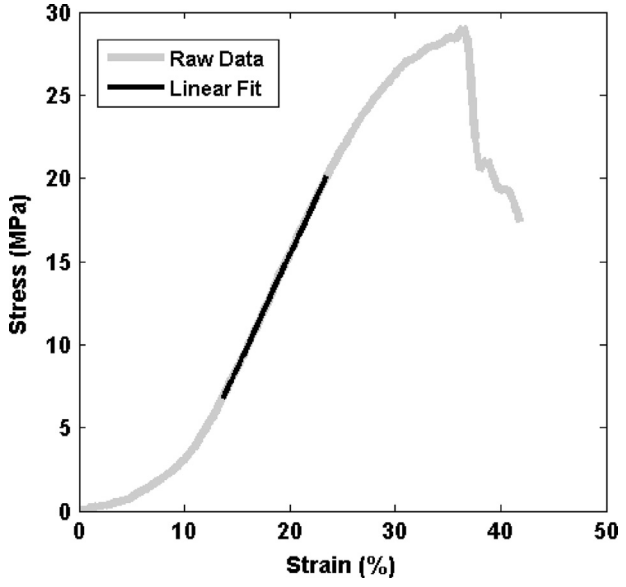

Fig. 3. A typical stress–clamp strain curve from a central band sample (C) taken from a left index finger extensor hood. The black line indicates the linear region where the tangent modulus was calculated. The corresponding tangent modulus is 133.9 MPa, yield stress is 29.0 MPa, and yield strain is 36%.

Values for the samples taken from the central axis of the extensor mechanism (locations A–E, Fig. 1), which carries the majority of the force, were used in further statistical tests of variations in mechanical properties along the extensor hood. First, potential differences in mechanical properties between specimens from different digits were examined. To minimize risk of a type II error (failing to detect a significant effect of digit when it existed), separate univariate analysis of variance (ANOVA) was performed for each dependent variable. Failure to detect any significant effect of digit led to subsequent grouping of the specimens in further testing examining the influence of specimen location within the extensor hood. The main effect of location was then tested with an ANOVA for the dependent variables ultimate strain and load, tangent modulus, linear stiffness, and thickness, respectively. Finding of a significant effect led to post-hoc Tukey's HSD tests to compare the influence of the different locations. These statistical analyses were performed using JMP version 10 (SAS Institute Inc., Cary, NC). In cases where the assumption of homogeneity of variance was invalid, Welch-ANOVA was employed instead of ANOVA and post-hoc testing was conducted with Games–Howell in SPSS version 22 (IBM, Armonk, NY, USA). The statistical significance level was set at 0.05 for all tests.

3. Results

A linear portion of the stress–strain curve could be found for each sample for computation of the tangent modulus, such that $R^2 > 0.98$ for the fit of the modulus for each sample (see Fig. 3).

ANOVA analysis showed no significant effects of digit (index/middle) on any of the mechanical property variables by finger type ($p > 0.05$ for each test). Thus, data from both digits were combined for subsequent assessment of the effect of specimen location within the extensor mechanism (Table 1). Univariate ANOVAs were performed on the dependent variables local tangent modulus, ultimate strain, ultimate load, and linear stiffness. Welch-ANOVA was performed on the clamp modulus and thickness data because they had non-uniform variance according to Levene's equal variance test.

The depth of the extensor mechanism varied significantly (Welch-ANOVA: $p < 0.001$) from the proximal to the distal sites (Table 1). The thickest part of the specimens was found near the MCP joint. The average thickness was 2.23 ± 0.57 mm (mean $\pm$ standard deviation) just proximal to the MCP joint (see Fig. 1, location A) and 2.21 ± 0.54 mm above the MCP (location B). The thickness of the extensor tendon decreases in its more distal sections. At the terminal slip (E), the extensor mechanism is less than half of the thickness at the MCP (1.07 ± 0.20 mm). Games–Howell multiple comparisons showed that the thicknesses of the specimens proximal to and above MCP (A and B) were significantly larger than in the central band, central slip and terminal slip (C, D, and E, respectively; see Table 1).

Ultimate load decreased in a corresponding manner (ANOVA: $p = 0.006$) along the tendon from proximal to distal sites (Table 1). The samples just proximal to MCP (A) had maximal ultimate loads of 96.0 ± 29.7 N, while the samples from the terminal slip (E) had ultimate loads of only 36.6 ± 25.2 N. Comparisons of particular locations revealed that the ultimate load of the specimens around the MCP joint (A and B) was significantly larger than at the terminal slip (E), (Tukey: $p < 0.05$). Ultimate clamp strain also varied significantly with location (ANOVA: $p = 0.038$), with a low value of $28 \pm 7\%$ at the central and terminal slips (D and E) and higher values of $35 \pm 11\%$ and $39 \pm 7\%$ near the MCP (A and B). Ultimate local strain showed a similar pattern but the effect of location was not significant (ANOVA: $p = 0.18$).

The clamp tangent modulus also varied significantly across the extensor mechanism (Welch ANOVA: $p = 0.009$). The Games–Howell test revealed significantly different values at the central band (C) and MCP joint (B). The modulus value almost doubled from 53.2 ± 21.2 MPa at the MCP joint (B) to 100.6 ± 50.8 MPa at the central band (C) and100.8 ± 46.8 MPa at the central slip (D). The differences are readily apparent visually as well as the slopes in the stress–strain curves (Fig. 4). Values for the local tangent modulus were on average 23% larger than the values for the clamp

Table 1
Mechanical properties computed from failure test: mean ± standard deviation.

Sample location	Clamp		Local		Linear stiffness (N/mm)	Ultimate load (N)*	Thickness (mm)*
	Tangent modulus (MPa)*	Ultimate strain (%)*	Tangent modulus (MPa)	Ultimate strain (%)			
Proximal to MCP (A)	76.22 ± 24.53 (n=7)	39 ± 7 (n=7)	89.44 ± 54.50 (n=5)	36 ± 14 (n=5)	55.47 ± 15.13 (n=7)	96.00 ± 29.66 (n=7)	2.23 ± 0.57 (n=7)
Over MCP (B)	53.16 ± 21.24 (n=12)	35 ± 11 (n=12)	81.99 ± 43.86 (n=12)	30 ± 12 (n=12)	44.38 ± 14.83 (n=12)	77.96 ± 33.96 (n=12)	2.21 ± 0.54 (n=12)
Central band (C)	100.61 ± 50.82 (n=13)	33 ± 10 (n=13)	114.03 ± 61.34 (n=10)	31 ± 11 (n=10)	45.84 ± 26.17 (n=13)	63.74 ± 33.69 (n=13)	1.38 ± 0.29 (n=13)
Central slip (D)	100.76 ± 46.77 (n=11)	28 ± 7 (n=11)	125.31 ± 62.06 (n=10)	23 ± 8 (n=10)	39.72 ± 23.11 (n=11)	57.60 ± 40.61 (n=11)	1.20 ± 0.31 (n=11)
Terminal slip (E)	89.67 ± 48.29 (n=11)	28 ± 7 (n=11)	96.97 ± 51.29 (n=11)	27 ± 9 (n=11)	29.71 ± 17.84 (n=11)	36.55 ± 25.23 (n=11)	1.07 ± 0.20 (n=11)
Sagittal band (F)	54.68 ± 14.13 (n=4)	30 ± 7 (n=4)	64.87 ± 29.30 (n=3)	26 ± 4 (n=3)	20.62 ± 16.71 (n=4)	27.97 ± 26.27 (n=4)	1.19 ± 0.33 (n=4)
Lateral band (G)	105.38 ± 85.06 (n=7)	33 ± 10 (n=7)	157.02 ± 138.37 (n=7)	26 ± 16 (n=7)	27.62 ± 15.89 (n=7)	53.32 ± 31.51 (n=7)	1.20 ± 0.39 (n=7)

n: number of the samples used to calculate the corresponding value. Data from index and middle fingers are combined.

* Significant difference among locations A–E, ($p < 0.05$).

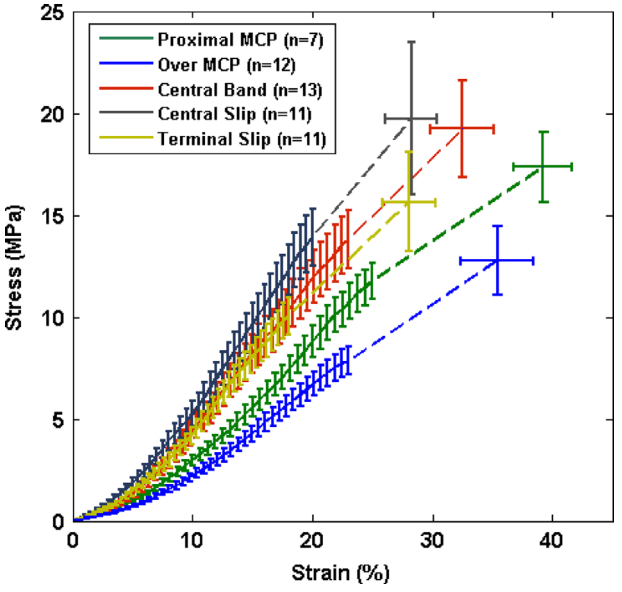

Fig. 4. Mean (± standard error) stress values for the given clamp strain percentages for each of the 5 locations along the central axis of the extensor hood. Crosses indicate point of ultimate stress (vertical bars indicate ± one SE) and ultimate percent strain (horizontal bars indicate ± one SE). n=number of samples used to compute values.

modulus, but the pattern was very similar. The local modulus ranged from 82.0 ± 43.9 MPa at the MCP (B) to 125.3 ± 62.1 MPa at the central slip (D). While the clamp tangent modulus changed significantly with sample location, the linear stiffness did not (ANOVA: p=0.12). The mean linear stiffness at the terminal slip (E: 29.7 ± 17.8 N/mm), however, was substantially smaller than the value at the location proximal to the MCP (A: 55.5 ± 15.1 N/mm). Unlike for the modulus values, the linear stiffness values from over the MCP, the central band, and the central slip were quite similar.

Samples from the sagittal band tended to be much more compliant than those for other locations (see Table 1). The mean values for the linear stiffness and ultimate load were the smallest for all of the sampled extensor hood locations. In contrast, the lateral band tended to be much stiffer, with an ultimate load double that of the sagittal band.

4. Discussion

Mechanical properties of the extensor mechanism were evaluated in different digits and at different locations along the structure. For the locations along the central axis of the extensor apparatus, ranging from the MCP joint to the terminal insertion site, mechanical properties did not vary significantly between the index and middle fingers. The thickness, stiffness, and ultimate strain were all very similar across the two digits and, thus, the samples could be grouped to focus on the main effect of location within the extensor mechanism.

Properties did vary significantly within the structure, however, location within the extensor hood had statistically significant effects on hood thickness, ultimate load, ultimate strain, and clamp tangent modulus. The thickness of the hood, for example, was greatest in the vicinity of the MCP joint and decreased distally, being smallest at the terminal slip. The thickness of the terminal slip was only half of that of the structures at the MCP joint. Accordingly, ultimate load was largest at the MCP joint and decreased as a function of distal position along the extensor apparatus. In contrast, the clamp and local tangent moduli tended to be larger at the distal sites (central band, central slip, and terminal slip), while smaller at the proximal sites (proximal MCP and over MCP). The greater stiffness may be needed to accommodate the loads transmitted to the insertion sites without causing excessive stretch of the tissue. Indeed, ultimate strain was the greatest in the most proximal regions of the extensor apparatus.

We also computed the linear stiffness to compare structural properties among different regions while accounting for the different thicknesses of the extensor hood in those regions. Linear stiffness did not vary significantly; the values through the middle of the structure from the MCP joint to the central slip were quite similar, much more so than the clamp tangent modulus. The mean linear stiffness for the terminal slip, however, was considerably smaller than the mean values for the other locations. Linear stiffness values were also relatively small in the lateral and sagittal bands. These differences in linear stiffness may be important in determining the relative force distribution between the central and terminal slips. This distribution, previously examined in cadaver specimens (Lee et al., 2008a; Valero-Cuevas et al., 2007), is a key parameter for computational modeling of the extensor apparatus. The linear stiffness values that we estimated were much smaller than those reported previously (Garcia-Elias et al., 1991b), for example, the mean stiffness over the MCP region was 256 N/mm, over the central band was 126 N/mm, and over the central slip was

294 N/mm. We believe that our values may be smaller due to the different method used to obtain the data. While we measured the elasticity in individual localized pieces of the hood, mechanical testing was done on the entire structure in the prior study. Linear stiffness was estimated from the local strain and the load force applied at two ends of the extensor apparatus. Thus, their bands were up to 5 times greater in cross-sectional area than ours, which were only 2 mm in width, with a resulting greater linear stiffness. In addition, in their preparation forces between the extensor hood and other structures, such as the joint capsule, may have reduced the net force applied to the tissue of interest and led to the appearance of greater stiffness.

Overall, the tangent moduli were small in comparison with reported values for other human tendons or ligaments (Stabile et al., 2004; Stäubli et al., 1999; Wren et al., 2001). For example, the clamp tangent modulus in our extensor hood specimens was almost an order of magnitude lower than values recorded from samples of the Achilles tendon (Wren et al., 2001), and less than one-third of the values reported for the anterior (Butler et al., 1986) and medial (Quapp and Weiss, 1998) collateral ligaments in the knee. While the elastic moduli of the extensor hood were much smaller than those reported for several other tendons and ligaments, ultimate strains were much larger. Ultimate clamp strain values of 28–39% and local strain values of 23-36% were obtained at the ultimate load. These values are two times higher than the ultimate strains reported for the Achilles tendon (Wren et al., 2001), the ACL (Butler et al., 1986), and the MCL (Quapp and Weiss, 1998). The seemingly greater elasticity of the extensor apparatus is needed to accommodate flexion of the finger joints. Strains of 2–3% in the extensor hood were recorded due to passive flexion alone of the fingers, without any applied tendon load (Lee et al., 2008a). Alternatively, possible differences among the studies in ages of the donors could also have impacted the observed elasticities (Noyes and Grood, 1976). Unfortunately, age and gender data were unavailable for the specimens used in this study.

In summary, in agreement with Landsmeer (1949), we saw variation in the mechanical characteristics of the extensor apparatus, although it is difficult to compare the absolute values we obtained with the previous study. While significant variations were not observed between the extensor hoods for different fingers, variations were observed throughout the structure for a given digit. Thickness and ultimate load were much greater in the proximal regions, but tangent modulus was larger in the more distal regions. Thus, the proximal regions were more compliant and, in fact, could withstand greater strain prior to failure.

The relative differences in mechanical properties throughout the extensor hood may substantially impact how force is transmitted through the structure. Our preliminary efforts to model this transmission with a finite element model of the extensor apparatus and underlying phalanges have suggested that load transfer from the tendons to the insertion sites in the central and terminal slips is significantly affected by the relative material properties throughout the structure. The specific contributions of the material properties and boundary conditions on the resulting forces at the terminal and central slips are a focus of further research by the authors. The variability in mechanical properties may have direct ramifications for surgical repair of extensor hood injuries, such as fixed boutonniere deformity (Littler and Eaton, 1967; Matev, 1969), especially in procedures for which grafts from areas in the extensor hood are used. In addition, they can inform the development of biomimetic robots, such as the ACT Hand (Deshpande et al., 2013).

Conflict of interest

All authors of this manuscript have no conflicts of interest to declare.

Acknowledgments

The authors would like to thank Dr. Vincent Wang and his laboratory staff from the Rush University Medical Center for providing expert advice regarding methodology and Dr. Joseph Towles for his assistance in acquiring specimens. This work was supported by Grant 1R01NS052369-01A1 from the National Institutes of Health (National Institute of Neurological Disorders).

References

An, K.N., Ueba, Y., Chao, E.Y., Cooney, W.P., Linscheid, R.L., 1983. Tendon excursion and moment arm of index finger muscles. J. Biomech. 16, 419–425.
Butler, D.L., Grood, E.S., Noyes, F.R., Zernicke, R.F., Brackett, K., 1984. Effects of structure and strain measurement technique on the material properties of young human tendons and fascia. J. Biomech. 17, 579–596.
Butler, D.L., Kay, M.D., Stouffer, D.C., 1986. Comparison of material properties in fascicle-bone units from human patellar tendon and knee ligaments. J. Biomech. 19, 425–432.
Deshpande, A.D., Xu, Z., Weghe, M.V., Brown, B.H., Ko, J., Chang, L.Y., Wilkinson, D. D., Bidic, S.M., Matsuoka, Y., 2013. Mechanisms of the anatomically correct testbed hand. IEEE/ASME Trans. Mechatron. 18, 238–250.
Doyle, J.R., 1988. Anatomy of the finger flexor tendon sheath and pulley system. J. Hand Surg. Am. 13, 473–484.
Garcia-Elias, M., An, K.-N., Berglund, L., Linscheid, R.L., Cooney Iii, W.P., Chao, E.Y.S., 1991a. Extensor mechanism of the fingers. I. A quantitative geometric study. J. Hand Surg. 16, 1130–1136.
Garcia-Elias, M., An, K.-N., Berglund, L.J., Linscheid, R.L., Cooney, W.P., Chao, E.Y.S., 1991b. Extensor mechanism of the fingers. II. Tensile properties of components. J. Hand Surg. 16, 1136–1140.
Harrison, S.H., 1965. Swan's neck deformity of the fingers. Br. J. Plast. Surg. 18, 79–87.
Hurlbut, P.T., Adams, B.D., 1995. Analysis of finger extensor mechanism strains. J. Hand Surg. 20, 832–840.
Infantolino, B.W., Challis, J.H., 2010. Architectural properties of the first dorsal interosseous muscle. J. Anat. 216, 463–469.
Kamper, D.G., Fischer, H.C., Cruz, E.G., 2006. Impact of finger posture on mapping from muscle activation to joint torque. Clin. Biomech. (Bristol, Avon) 21, 361–369.
Kelleher, J.E., Siegmund, T., Chan, R.W., Henslee, E.A., 2011. Optical measurements of vocal fold tensile properties: implications for phonatory mechanics. J. Biomech. 44, 1729–1734.
Landsmeer, J., 1949. The anatomy of the dorsal aponeurosis of the human finger and its functional significance. Anat. Rec. 104, 31–44.
Lee, S.W., Chen, H., Towles, J.D., Kamper, D.G., 2008a. Effect of finger posture on the tendon force distribution within the finger extensor mechanism. J. Biomech. Eng. 130, 051014.
Lee, S.W., Chen, H., Towles, J.D., Kamper, D.G., 2008b. Estimation of the effective static moment arms of the tendons in the index finger extensor mechanism. J. Biomech. 41, 1567–1573.
Lemon, R., 1993. The G. L. Brown Prize Lecture. Cortical control of the primate hand. Exp. Physiol. 78, 263–301.
Littler, J.W., Eaton, R.G., 1967. Redistribution of forces in the correction of the Boutonnière deformity. J. Bone Jt. Surg. 49, 1267–1274.
Matev, I., 1969. The boutonniere deformity. Hand 1, 90–95.
Micks, J.E., Reswick, J.B., 1981. Confirmation of differential loading of lateral and central fibers of the extensor tendon. J. Hand Surg. Am. 6, 462–467.
Milford, L.W., 1968. Retaining Ligaments of the Digits of the Hand: Gross and Microscopic Anatomic Study. W. B. Saunders Company, Philadelphia.
Mulder, J., Landsmeer, J., 1968. The mechanism of claw finger. J. Bone Jt. Surg. Br. 50, 664–668.
Noyes, F.R., Grood, E.S., 1976. The strength of the anterior cruciate ligament in humans and Rhesus monkeys. J. Bone Jt. Surg. Am. 58, 1074–1082.
Quapp, K.M., Weiss, J.A., 1998. Material characterization of human medial collateral ligament. J. Biomech. Eng. 120, 757–763.
Sabnis, A.S., 2013. Morphological study of cutaneous ligaments. Int. J. Anat. Physiol. 2, 11–13.
Sarrafian, S.K., Kazarian, L.E., Topouzian, L.K., Sarrafian, V.K., Siegelman, A., 1970. Strain variation in the components of the extensor apparatus of the finger during flexion and extension. A biomechanical study. J. Bone Jt. Surg. 52, 980–990.
Saxena, A., Lipson, H., Valero-Cuevas, F.J., 2012. Functional inference of complex anatomical tendinous networks at a macroscopic scale via sparse experimentation. PLoS Comput. Biol. 8, e1002751.
Stabile, K.J., Pfaeffle, J., Weiss, J.A., Fischer, K., Tomaino, M.M., 2004. Bi-directional mechanical properties of the human forearm interosseous ligament. J. Orthop. Res. 22, 607–612.
Stack, H.G., 1969. Mallet finger. Hand 1, 83–89.
Stäubli, H.U., Schatzmann, L., Brunner, P., Rincón, L., Nolte, L.-P., 1999. Mechanical tensile properties of the quadriceps tendon and patellar ligament in young adults. Am. J. Sports Med. 27, 27–34.

Tubiana, R., Valentin, P., 1964. The anatomy of the extensor apparatus of the fingers. Surg. Clin. North Am. 44, 897–906.
Valero-Cuevas, F., 2009. Why the hand?. In: Sternad, D. (Ed.), Progress in Motor Control. Springer, US, pp. 553–557.
Valero-Cuevas, F.J., Jae-Woong, Y., Brown, D., McNamara, R.V., Paul, C., Lipson, H., 2007. The tendon network of the fingers performs anatomical computation at a macroscopic scale. IEEE Trans. Biomed. Eng. 54, 1161–1166.
Valero-Cuevas, F.J., Zajac, F.E., Burgar, C.G., 1998. Large index-fingertip forces are produced by subject-independent patterns of muscle excitation. J. Biomech. 31, 693–703.
von Schroeder, H.P., Botte, M.J., 1993. The functional significance of the long extensors and juncturae tendinum in finger extension. J. Hand Surg. Am. 18, 641–647.
Winslow, J.B., 1732. Exposition Anatomique De La Structure Du Corps Humain. Guillaume Desprezet Jean Desessarte, Paris.
Woo, S., Gomez, M., Seguchi, Y., Endo, C., Akeson, W., 1983. Measurement of mechanical properties of ligament substance from a bone-ligament-bone preparation. J. Orthop. Res. 1, 22–29.
Wren, T.A., Yerby, S.A., Beaupré, G.S., Carter, D.R., 2001. Mechanical properties of the human Achilles tendon. Clin. Biomech. 16, 245–251.
Zancolli, E., 1979. Structural and Dynamic Bases of Hand Surgery. J. B. Lippincott, Philadelphia.